TECHNICAL PAPER

Influence of hardness and grain size of the SS431 material on the slurry erosion wear through the pot tester at higher slurry concentrations

Yatish Kumar Baghel[1] · Vivek Kumar Patel[2]

Abstract

One of the most crucial considerations when developing any slurry transportation system is evaluating slurry erosion because it significantly contributes to the system's many component's ineffective operation and eventual failure. In the present work, the impact of the thermo-mechanical process (TMP) on the resistance of the slurry erosion wear of the target material has been investigated at a high solid concentration (50–70% fly ash by weight) and different rotational speeds (300–600 rpm) of the specimen. SS431 was used as the target material, and the Gleebles® 3800 simulator was used to perform the TMP on the target material. In the Gleebles® 3800 simulator, four strain rates (0.01, 0.1, 1, and 10 s^{-1}) were used for the deformation at two temperatures (950 °C and 1050 °C). A slurry pot tester evaluated the slurry erosion wear for 15 h at room temperature. TMP specimens exhibit superior resistance to slurry erosion wear compared to as-received SS431 material at all flow parameters. The best resistance to slurry erosion was observed in specimens that had been TMP at 1050 °C with a strain rate of 1 s^{-1}. Correlations had been found between various target material properties (hardness and grain size) as well as flow properties (solid concentration and rotational speed of the specimens) and the slurry erosion wear, all of which contribute to the erosion mechanism.

Keywords Slurry erosion wear · Thermo-mechanical process · Fly ash · Stainless steel · Hardness

1 Introduction

Martensitic stainless steel (MSS) is a very versatile material that finds widespread use in several sectors due to its diverse range of applications. This sector includes the desalination of seawater, various industries (paper, chemical, food, petrochemical), shipbuilding, slurry transportation in thermal power plants and shipbuilding [1–3]. Cast SS431 MSS has emerged as a notable choice for specific applications, particularly in constructing slurry transportation systems (STS) and hydropower plants among the varieties of martensitic stainless steel. This preference is underpinned by the material's commendable corrosion resistance and remarkable mechanical characteristics, which make it well-suited for these demanding environments [1, 4, 5]. The solid particles constantly attack the blade, pump casing, bend joints and other STS components and are subject to erosion wear; the hardness of the erodent particles has influenced that slurry erosion wear during the slurry transportation process [4, 6, 7]. This slurry erosion has far-reaching effects. Based on the solid concentration, STS has three types: low (10–20% solid by weight), medium (30–40% solid by weight), and high (> 50% solid by weight) concentration disposal systems [8]. The STS's overall effectiveness decreases when the material eventually leads to erosion wear, which could result in deterioration in specific components. This problem highlights how urgently the slurry erosion resistance of the SS431 material has to be improved. Over time, numerous endeavors have been launched to tackle this challenge. These efforts encompass an array of strategies, such as subjecting

✉ Vivek Kumar Patel
  vivek@mnnit.ac.in

  Yatish Kumar Baghel
  yatishbaghel@gmail.com

1 Mechanical Engineering Department, Invertis University, Bareilly, Uttar Pradesh 243123, India

2 Department of Applied Mechanics, Motilal Nehru National Institute of Technology Allahabad, Prayagraj, Uttar Pradesh 211004, India

Table 1 Chemical composition (in % weight) of the SS431

| Material	Cr	Ni	Mn	C	Si	P	Fe
SS431	17.878	2.023	0.986	0.165	0.406	0.019	80.175
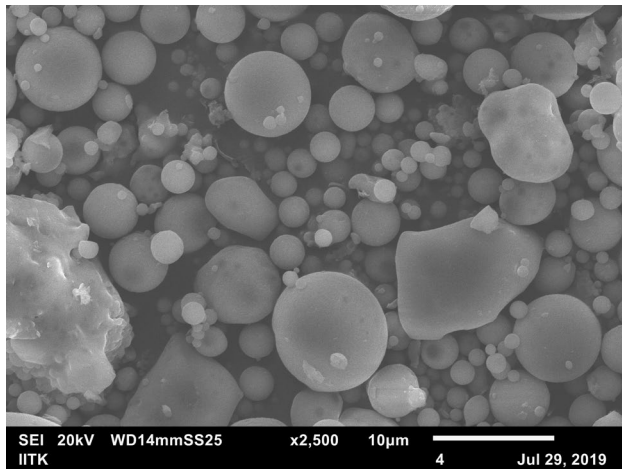
Fig. 1 SEM of the erodent particles

the material to heat treatments in order to modify its properties [9], applying various types of coatings to enhance its surface characteristics [10–13], employing laser transformation hardening (LTH) process due to which the hardness of the material has been improved [14], and adopting the friction stir processing (FSP) technique to induce specific improvements in the hardness and refine the microstructure of the material [15, 16]. However, it is essential to acknowledge that the use of surface modification techniques comes with its own set of drawbacks. These include the potential for porosity within the modified surfaces, issues related to inadequate adhesion, the introduction of dilution effects, and the uneven distribution of microstructural changes [17]. The MSS's effectiveness against erosion has been hampered because of this.

The cyclic heat treatment process through the thermal–mechanical process was applied to the material (13Cr–4Ni), and the slurry erosion wear was investigated. They found that the cyclic heat-treated material's wear resistance properties have increased compared to the as-received material [18]. Forging (multidirectional) and annealing processes have been applied to the HSLA material to change the material's mechanical properties. After that, slurry erosion wear was found at different flow conditions with the help of a pot tester [19]. In that investigation, an Ultrasonic vibration-based experimental setup was also used to investigate the cavitation wear of the HSLA material. They found that the high hardness and toughness of the processed HSLA material resulted in more effective erosion resistance to the as-received material.

Two methods: Focused ion beam (FIB) as well as transmission electron microscopy (TEM) have been utilized to improve the properties of the target material (SS316) and analyze the erosion and erosion–corrosion of the target material, and also observe the effect of microstructure of the material on both erosions as well as erosion–corrosion wear at different operation conditions [20]. For slurry erosive wear to occur, the hardness of the solid particles must be higher than that of the target material [21]. The hardness and ductility of a material are a crucial factor in determining its resistance to erosion wear, as indicated by studies [22–28].

Thermo-mechanical processing (TMP) is an additional possibility in the context of metal processing. Processes such as work hardening, dynamic recovery, and dynamic recrystallization cause a variety of changes in microstructure [29]. It can change the mechanical characteristics that affect the resistance to slurry erosion. The economic enhancement of slurry erosion resistance in SS431 can be achieved through the use of TMP. This is due to the fact that the steel's
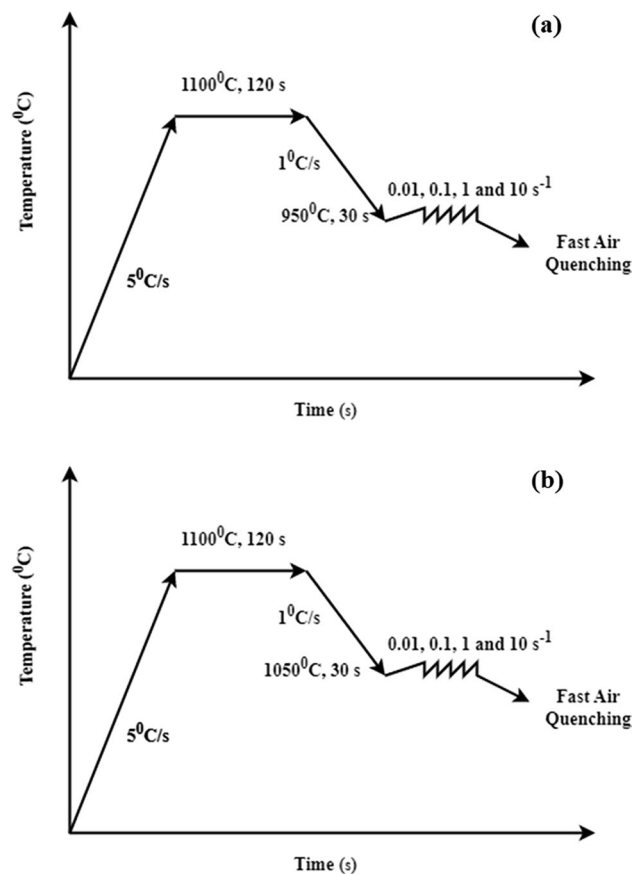
Fig. 2 TMP Schedule of SS431 for hot deformation at **a** 950 °C, **b** 1050 °C
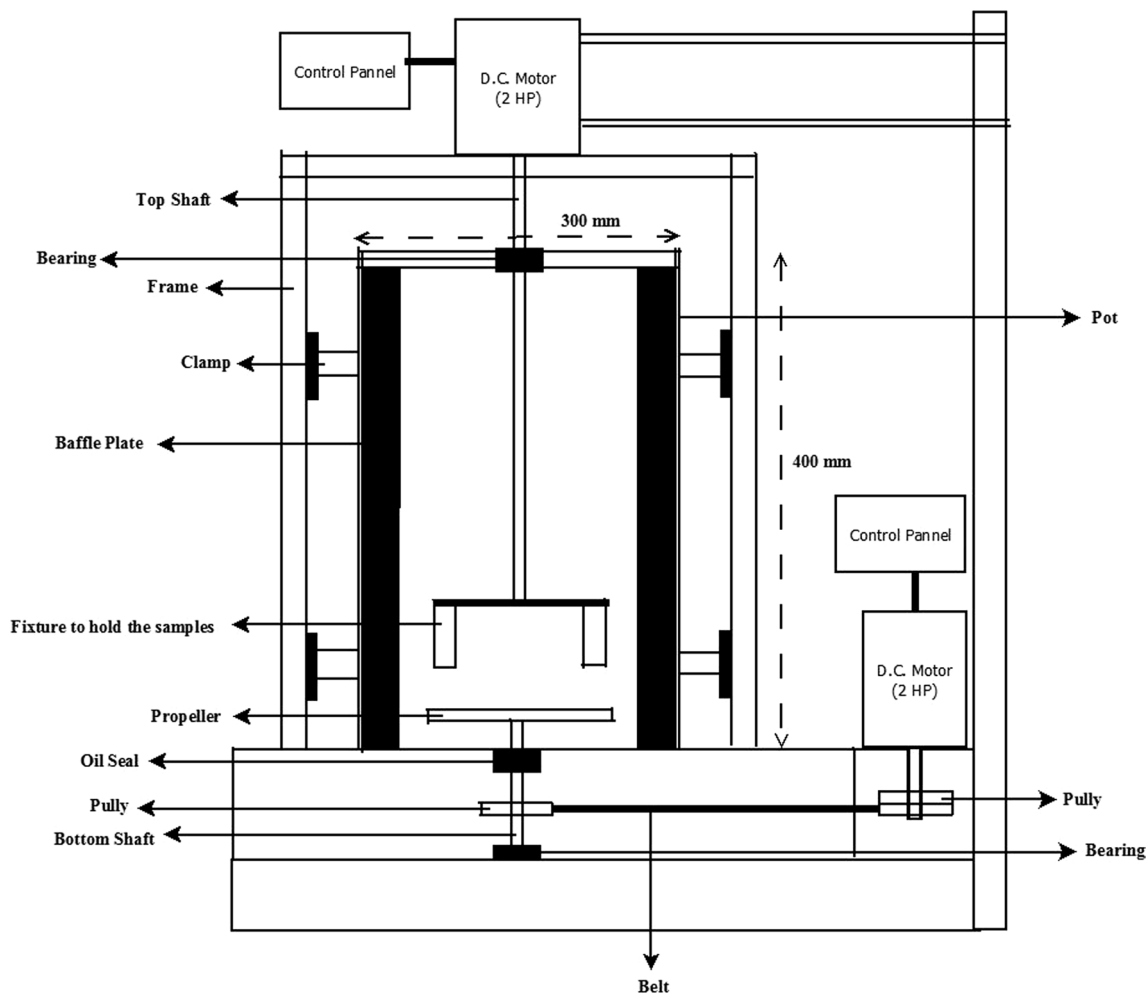
Fig. 3 Schematic line diagram of experimental setup for slurry erosion wear

beneficial hardness and erosion resistance are derived from the change of hardness as well as microstructures [15].

Hence, the aim of this study is to examine the impact of TMP on the slurry erosion resistance of SS431 at two different deformation temperatures, namely 950 °C and 1050 °C, and four distinct strain rates of 0.01, 0.1, 1, and 10 s^{-1} at high solid concentration of the slurry (50–70% fly ash by weight) and different rotational speeds (300–600 rpm) of the specimens. The erosion wear resistance in the as-received material was compared with the processed materials (TMP specimens). The mechanical properties (hardness and grain size) as well as flow properties (solid concentration and rotational speed) of the SS431 material have been observed in correlation with the slurry erosion wear.

2 Material and methods

2.1 Target material and erodent particles

The ingot of SS431 in the form of an 18 mm diameter was provided by M/s special Metals, Mumbai, India. The details of the chemical compositions (Table 1) of the SS431 material were provided by the Real Metal Test Laboratory in Mumbai, India. In accordance with the requirements of standard ASTM E209 [30], the specimens for the thermomechanical process have been prepared from SS431 ingots of 15 mm in height and 10 mm in diameter through the Wire Cut Electro-Discharge Machine (EDM).

Fly ash has been used as an erodent particle which has been procured from the Prayagraj Power Generation Company Limited (PPGCL), Prayagraj, Uttar Pradesh. A scanning electron microscope (SEM) has been utilized to observe the shape of the fly ash particles, as shown in Fig. 1.
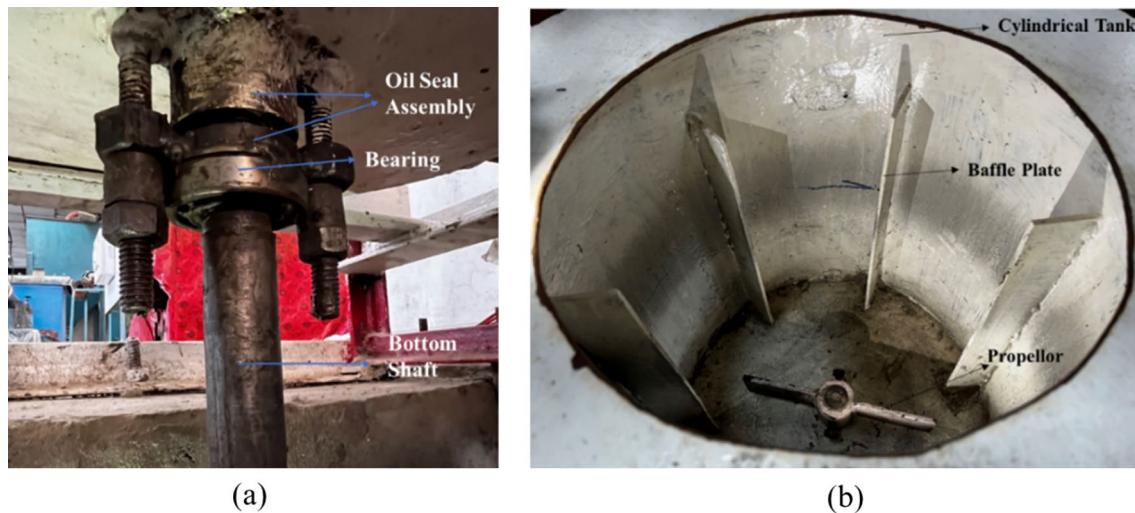
Fig. 4 **a** Oil seal assembly, **b** cylindrical tank with baffle plate and propellor

2.2 Mechanical process and characterization

Various studies have described the guideline for the heat treatment procedure that should be carried out for the SS431 martensitic stainless steel [31–33], and these studies observed that austenitization temperatures range for the SS431 martensitic stainless steel should be in the range of 950 °C to 1150 °C, as it aids in dissolving carbides and reduces the amount of ferrite. In order to simulate hot deformation, a thermo-mechanical simulator (Gleeble® 3800) was used, and this testing was performed in the Department of Metallurgical and Materials Engineering,

IIT Roorkee. Graphite was used to lubricate the end surfaces of the cylindrical specimens, and a thermocouple was a spot welded in the middle of each one. When the temperature was raised, tantalum foils were able to prevent the specimen and the anvil from sticking together. The intended thermo-mechanical process (TMP) cycles are schematically depicted in Fig. 2.

Homogenization of the samples involved heating them from 5 °C/s to 1100 °C and holding them there for 120 s. In order to reach the temperature at which the specimens deformed, they were chilled at a rate of 1 °C/s. A dwell time of thirty seconds was included in order to get rid of
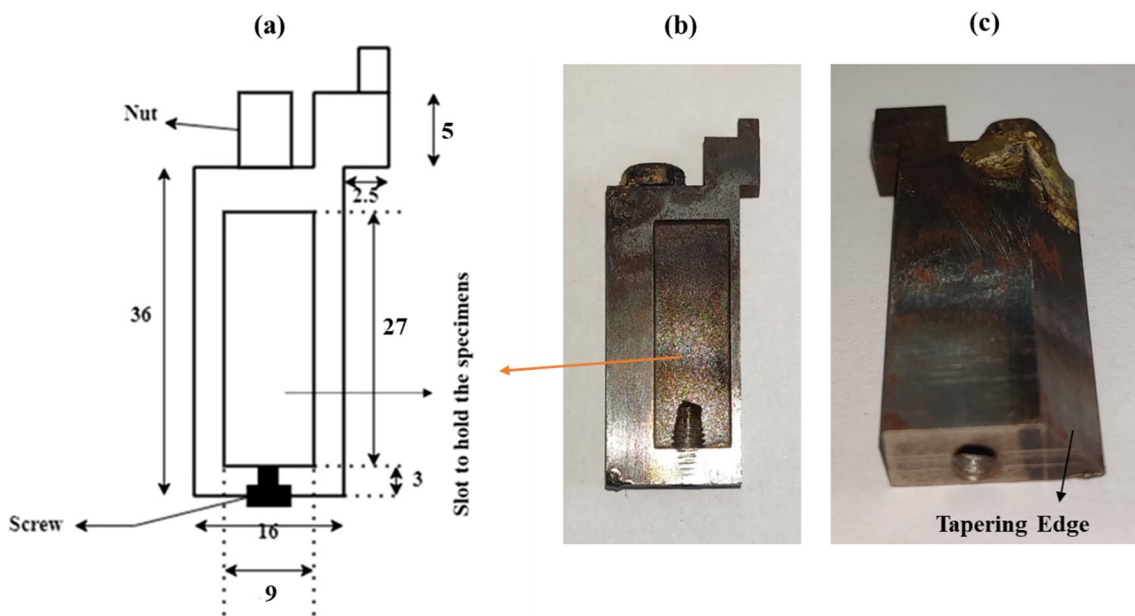

Fig. 5 Test fixture. **a** Schematic line diagram. **b** Actual fixture. **c** Back side of the fixture

any thermal gradients that may have been present. Two different temperatures of deformation, 950 and 1050 °C, corresponding to four different strain rates, 0.01, 0.1, 1, and 10 s^{-1}, have been selected for this experiment. In this analysis, the specimens have been compressed throughout their length by fifty percent. The examination of the evolution of microstructure is made possible by a rapid air quenching.

An optical microscope (Make: 1810, OMNITECH) has been used for the purpose of microstructural characterization. In order to prepare the specimen for microscopic inspection, the surface of the as-received (ASR) specimen and TMP specimens are prepared with the help of a polishing machine using different grades of emery papers (grade 180, 200, 400, 600, 800, 1000, 1200, 1500 and 2000) followed by wet cloth polishing with a 0.02 μm grade alumina powder. The specimen's polished surfaces were electroetched using a solution of cupric chloride (1.5 gm), nitric acid (33 ml), Ethanol (33 ml), and distilled water (33 ml) for microstructural examination. Vickers micro-hardness tester (Make: RADICAL) with a 10 kg load and 15 s dwell time has been used to assess the micro-hardness of polished surfaces. Hardness was calculated at ten different locations of the samples, and an average result was used.

2.3 Experimental setup for erosion wear and fixture

In the present work, erosion wear of the material has been carried out in an accelerated form with the help of a modified pot tester, and the effect of rotational speed of the specimen (as-received and TMP specimens) and solid concentration is analyzed on the slurry erosion wear. The reference design for the pot tester utilized in the present work is adopted from the previous studies [34, 35]. Figure 3 shows the schematic line diagram of the pot tester. A sheet (5 mm) of mild steel was used to make the pot tester's cylindrical tank (64.55 L), which was mounted on the frame with the help of clamps. The experimental setup is driven by two DC motors, each with a 2 HP power rating and 1500 rpm speed. In the experimental setup, two shafts (top and bottom shafts) have been coupled with the motors separately, as shown in Fig. 3. At a fixed distance, two rotating arms have

been used to hold the fixtures connected to the top shaft; while, the stirrer assembly is connected to the bottom shaft. A stirrer assembly is provided to avoid freezing the slurry. The bottom shaft (34 mm) is inserted from the bottom of the cylindrical tank, and the propeller is rotated with the help of a belt pulley arrangement. A bearing holds this shaft from inside the tank, which is supported by a frame. The rotational speed of the lower shaft varied from 50 to 100 rpm and was controlled by a control panel (speed controller). In the slurry erosion wear testing, the speed of the bottom shaft depends on the solid concentration to avoid settling the slurry. An oil seal is installed at the bottom of the tank along with the shaft to prevent slurry leakage during the pot tester operation, as shown in Fig. 4a. Due to the high proportion of fly ash (by weight percentage), stirrer motion is continuously maintained to ensure a uniform slurry concentration throughout the tank's height. This prevents the slurry from settling and maintains consistent conditions on the surfaces of the target material.

One motor was fixed on the frame, and the top shaft was connected to this motor. The top shaft (34 mm) has been used in order to convey motion from the 2 HP motor to the fixture's holding arm. The fixtures have been connected
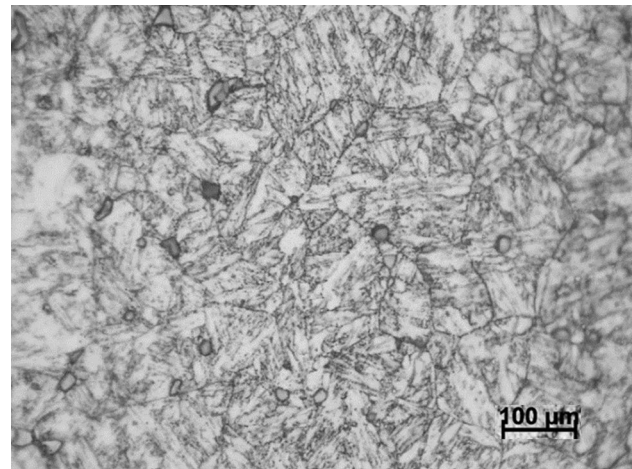

Fig. 6 Microstructure of the ASR sample

Table 2 Parameters for experimental analysis

Parameters	Details
Material	SS431
Erodent particle	Fly ash
Rotational speed of the fixture	300 to 600 rpm
Impact angle	90°
Solid concentration	50%, 60% and 70% by weight
Test duration	15 h

Table 3 Average grain size of TMP specimens at different deformation temperatures and strain rate

Strain rate (s^{-1})	Average grain size of hot deformed samples	
	950 °C	1050 °C
0.01	90.98 μm	75.86 μm
0.1	80.11 μm	63.75 μm
1	65.52 μm	51.12 μm
10	71.67 μm	63.52 μm
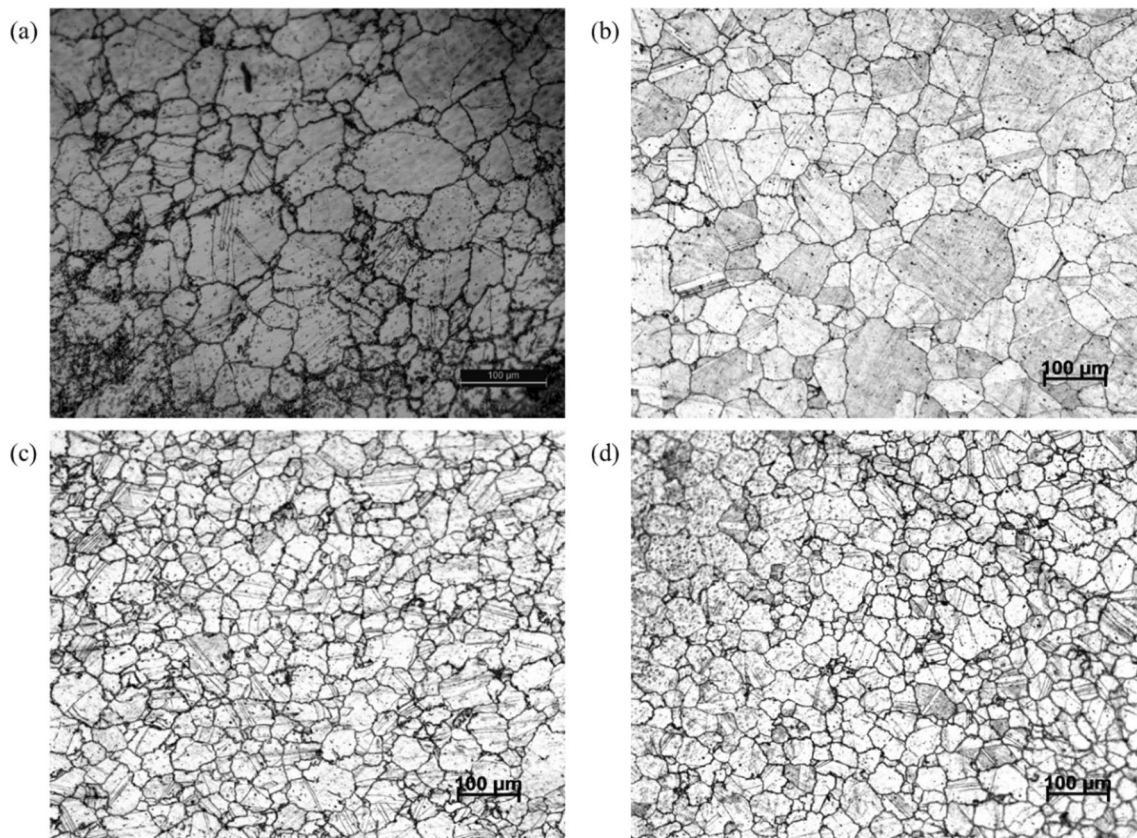
Fig. 7 Microstructure of the TMP sample at 950 °C for different strain rate. **a** 0.01 s^{-1}, **b** 0.1 s^{-1}, **c** 1 s^{-1} and **d** 10 s^{-1}

with the two rotating arms (75 mm long) connected to the sleeve. Bolts have been used to connect the sleeve to the top shaft. The top shaft was put into the tank from the top side, which was supported by a single bearing on the lid. The speed controller controls the speed of the top shaft, and it has been used in order to require the variable speed of the top shaft (300 rpm, 400 rpm, 500 rpm, and 600 rpm). Six U-shaped baffle plates have been attached to the pot tester wall (cylindrical tank), as shown in Fig. 4b, to disperse the vortex motion created by the propellor and the movement of the arms. After the experiment, the slurry was drained out from the tank with the help of a pipe connected at the bottom. During the subsequent round of tests, the lid is removed from the pot tester, allowing fresh slurry to be poured from the top after testing.

During slurry erosion testing, a fixture is required to hold the erosion wear specimens. Therefore, the fixtures are made from hardened steel (EN91) to minimize wear-related changes in their configuration. CNC machines have been used to fabricate the fixtures from hardened steel, and a groove has been made in the center with dimensions 27 mm × 9 mm × 2 mm to hold the samples for erosion wear testing. Figure 5a and b illustrate the schematic line diagram and actual photo of the fixture, respectively. In order

to reduce wake interference, only two fixtures have been provided, and these two fixtures are attached to the two arms (180° apart from the sleeve), as shown in Fig. 3. In order to prevent separation at the leading edge, the leading edges of the fixtures are changed by providing a tapering edge at an angle of 45° (Fig. 5c). Fixtures can be securely fastened to the arms with the help of a 5 mm nut located at the top of the test fixture. Wear specimens are inserted in the groove and tightened with the help of a screw.

2.4 Procedure and operating parameters for experimental analysis

As per fixture slot dimensions [27 mm × 9 mm × 2 mm], as-received (ASR) and processed materials have been cut through the wire EDM cut machine. Before pouring the fly ash slurry into the pot tester, the slurry for the experiment is made by combining the necessary quantity of fly ash and water to obtain the pre-decided concentration. During the experiments, the fixture was rotated at different rotational speeds with the help of the DC motor, and the control panel controlled that speed. All the experiments have been performed for 15 h.
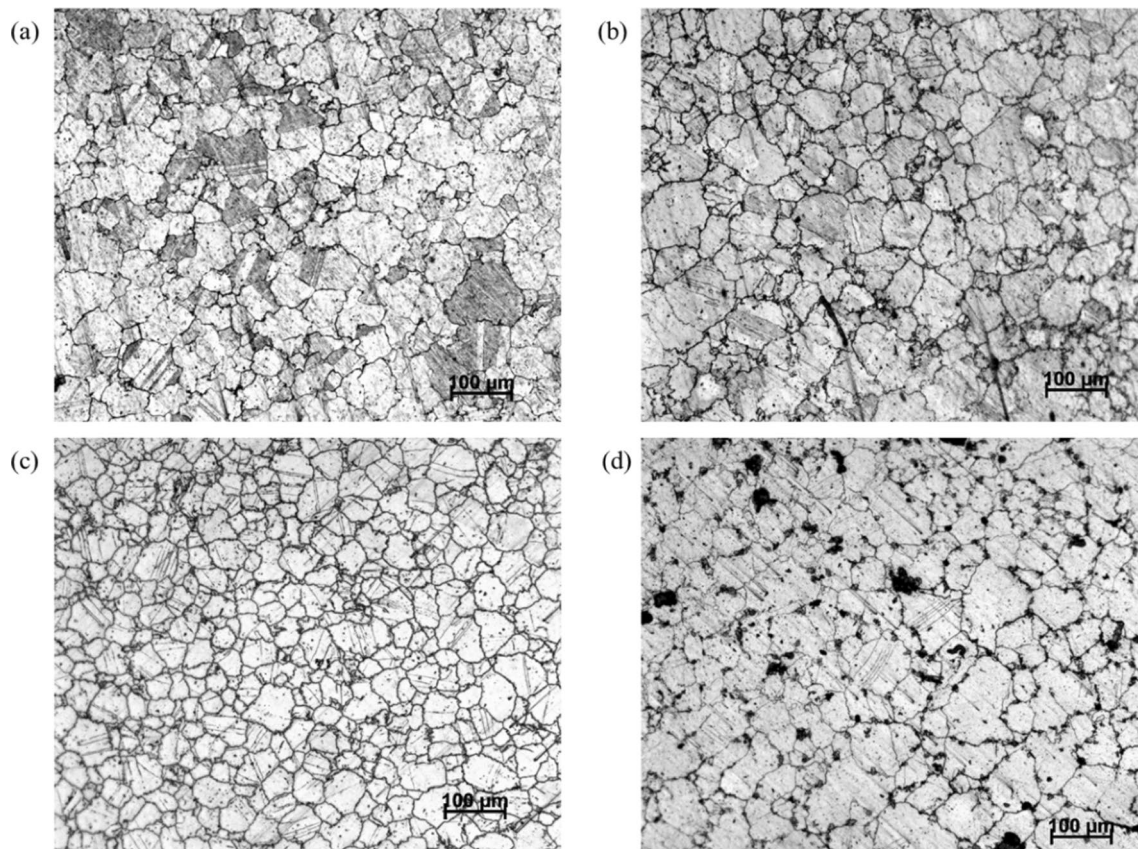
Fig. 8 Microstructure of the TMP sample at 1050 °C for different strain rate. **a** 0.01 s^{-1}, **b** 0.1 s^{-1}, **c** 1 s^{-1} and **d** 10 s^{-1}

Table 4 Hardness of the TMP specimens

Strain rate (s^{-1}) ↓	Temperature →	Hardness (Hv)	
		950 °C	1050 °C
0.01		462.26	470.55
0.1		481.725	485.075
1		486.675	492.84
10		471.72	475.54

After performing the experiments for all possible parameter combinations on the target specimens, erosion wear has been calculated by considering the average weight loss. In the interval of 3 h, any surface deposits on the wear specimens during the experimentation are removed by acetone. Any remaining water or acetone on the wear specimens is then blown off using a hot air blower. After being specimens dried in an oven (at 100 °C), samples were weighed on a weighing machine (Model CA-224D, CONTECH) with a ± 0.1 mg accuracy to determine the weight loss of the specimens. At every operating state, the variation in weight loss between the two specimens has been found to be within ± 2%.

Various flow parameters, such as the rotational speed of the fixture and solid concentration, have been selected to find the erosion wear of the various specimens (as-received and TMP) of the SS431 materials. Slurry erosion wear has been tested with a range of solid concentrations, from 50% by weight to 70% by weight, in the solid–liquid mixture. The impact angle is held constant at 90°; while, the fixture's rotational speed is changed from 300 to 600 rpm. Table 2 shows various parameters utilized for the experimental analysis.

3 Results and discussion

Experimental results have been obtained and analyzed in order to present a comparative description of the slurry erosion behavior of as-received (ASR) and thermo-mechanical processed specimens of SS431. A thorough discussion of how erosion wear depends on the target material's hardness, relative velocity, and solid concentration is provided in the following sections.
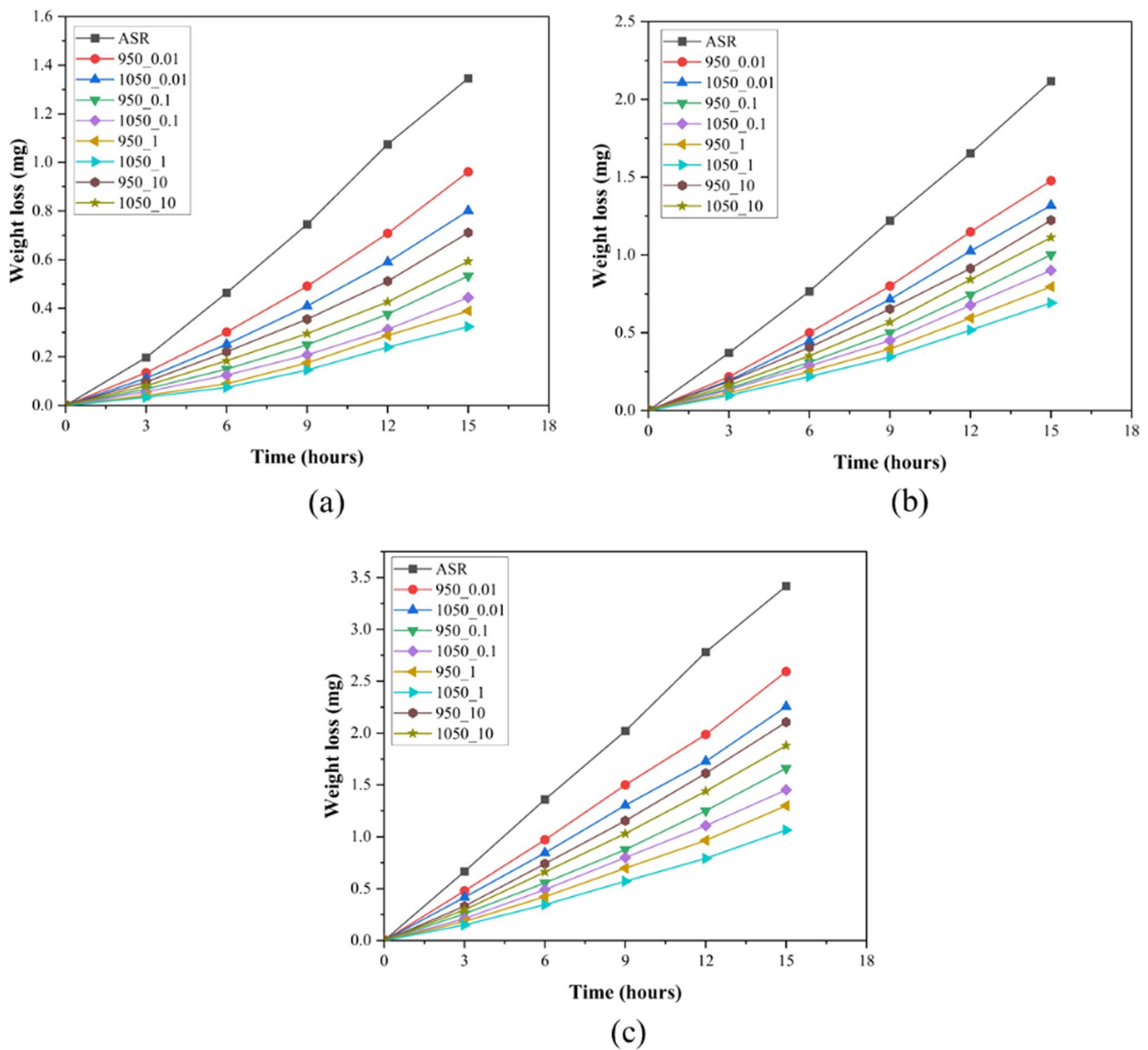
Fig. 9 Weight loss of the various specimens at 300 rpm. **a** 50%, **b** 60% and **c** 70% solid concentration (by weight)

3.1 Grain size and hardness of the specimens

Figure 6 shows a microstructure of the as-received (ASR) specimen and a 215.15 μm grain size has been found. At temperatures below 900 °C, the workability of the SS431 is greatly constrained [36, 37]. Thus, the thermo-mechanical process has been performed at 950 and 1050 °C

temperatures. Grain development became uncontrollable once temperatures reached 1050 °C and above [38]. Between the range of temperatures 950 and 1050 °C (austenitization temperature range), a metallurgical phenomenon like recovery and recrystallization occurs, which reduces the original austenite grain size and modifies the microstructures. The evolution of microstructure has been observed by
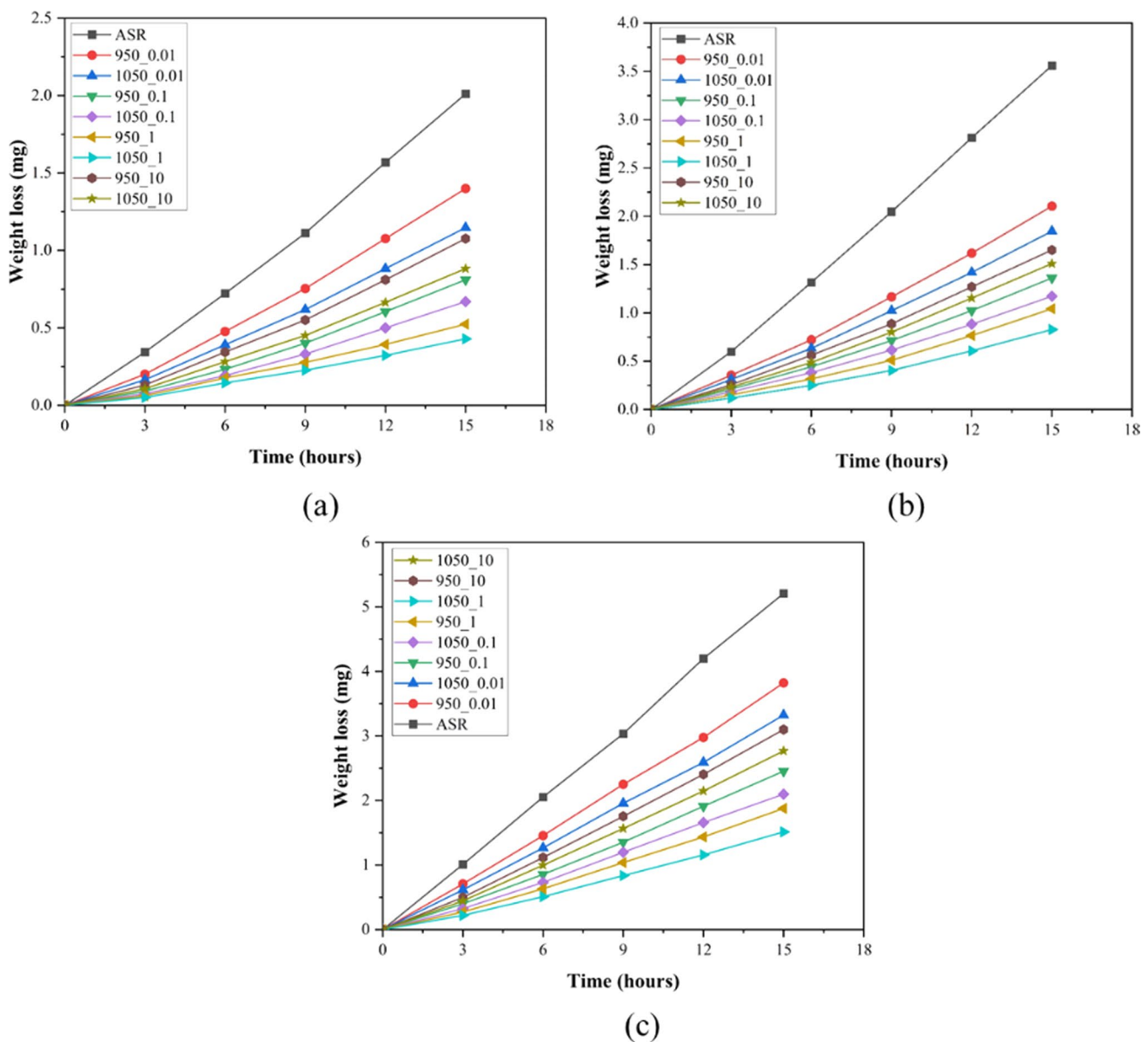
Fig. 10 Weight loss of the various specimens at 400 rpm. **a** 50%, **b** 60% and **c** 70% solid concentration (by weight)

considering the effect of lower and higher strain that is governed by a diffusional process and is influenced with time.

At different various strain rates, the average grain size of all processed specimens (TMP specimens) is shown in Table 3. The average grain size of all processed specimens is lower than that of the as-received specimen. The strain rates used to deform the TMP specimens at 950 and 1050 °C are depicted in the optical micrographs shown in Figs. 7, 8. In the hot deformation process, the large grains have broken due to recrystallization. Still, at the same time, there is sufficient time for recrystallization and dislocation movements at lower strain rates (0.01, 0.1, 1 s^{-1}). Hence, the grain size of the TMP specimens decreases up to 1 s^{-1} strain rate due to

the generation of new smaller grains, as shown in Figs. 7a–c and 8a–c. There is a lack of time for recrystallization in the case of higher strain rates (10 s^{-1}). In contrast, large grains are still broken but couldn't be reduced further due to less time for recrystallization; hence, the new smaller grains are absent or significantly less, as shown in Figs. 7d and 8d with respect to a more significant number of new smaller grains are visible at low strain rate for both deformation temperatures. Therefore, the grain size is increased at 10 s^{-1} strain rates as compared to 1 s^{-1} strain rate at both deformation temperatures.

A hardness test is performed with the help of a Vickers micro-hardness tester to determine the hardness of
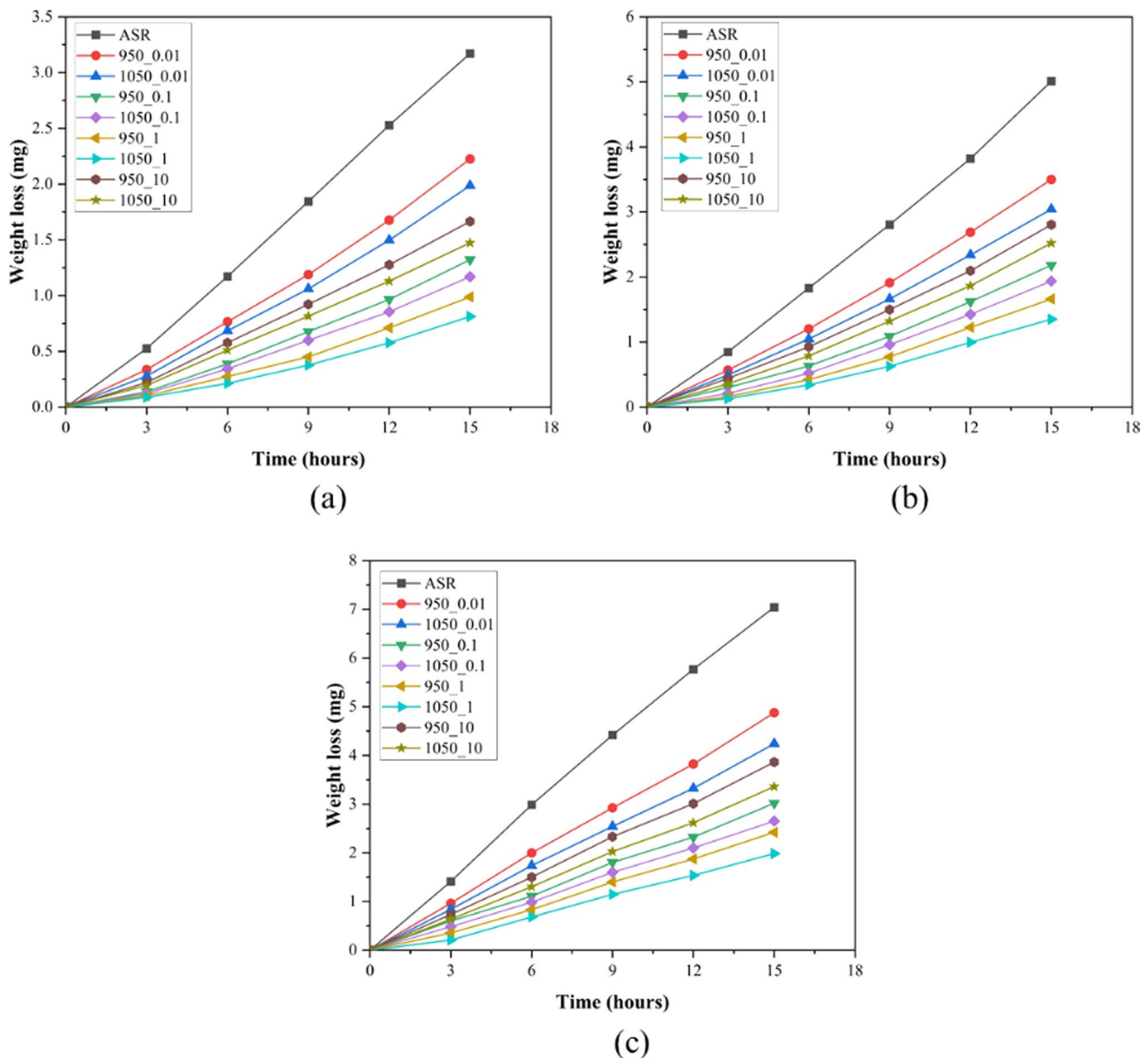
Fig. 11 Weight loss of the various specimens at 500 rpm. **a** 50%, **b** 60% and **c** 70% solid concentration (by weight)

as-received and TMP specimens. The average hardness of ASR SS431 is 298.83 Hv. Table 4 shows the hardness of TMP specimens at different deformation temperatures and strain rates. It has been found that the TMP specimens have the highest hardness compared to the ASR specimen. In TMP specimens, the hardness increases with the rise in deformation temperature. The TMP specimen exhibited the highest average hardness at 1050 °C, 1 s^{-1}. The hardness of the TMP specimen (1050 °C, 1 s^{-1}) is increased by 1.79 times and 1.02 times as compared to ASR and other TMP specimens, respectively.
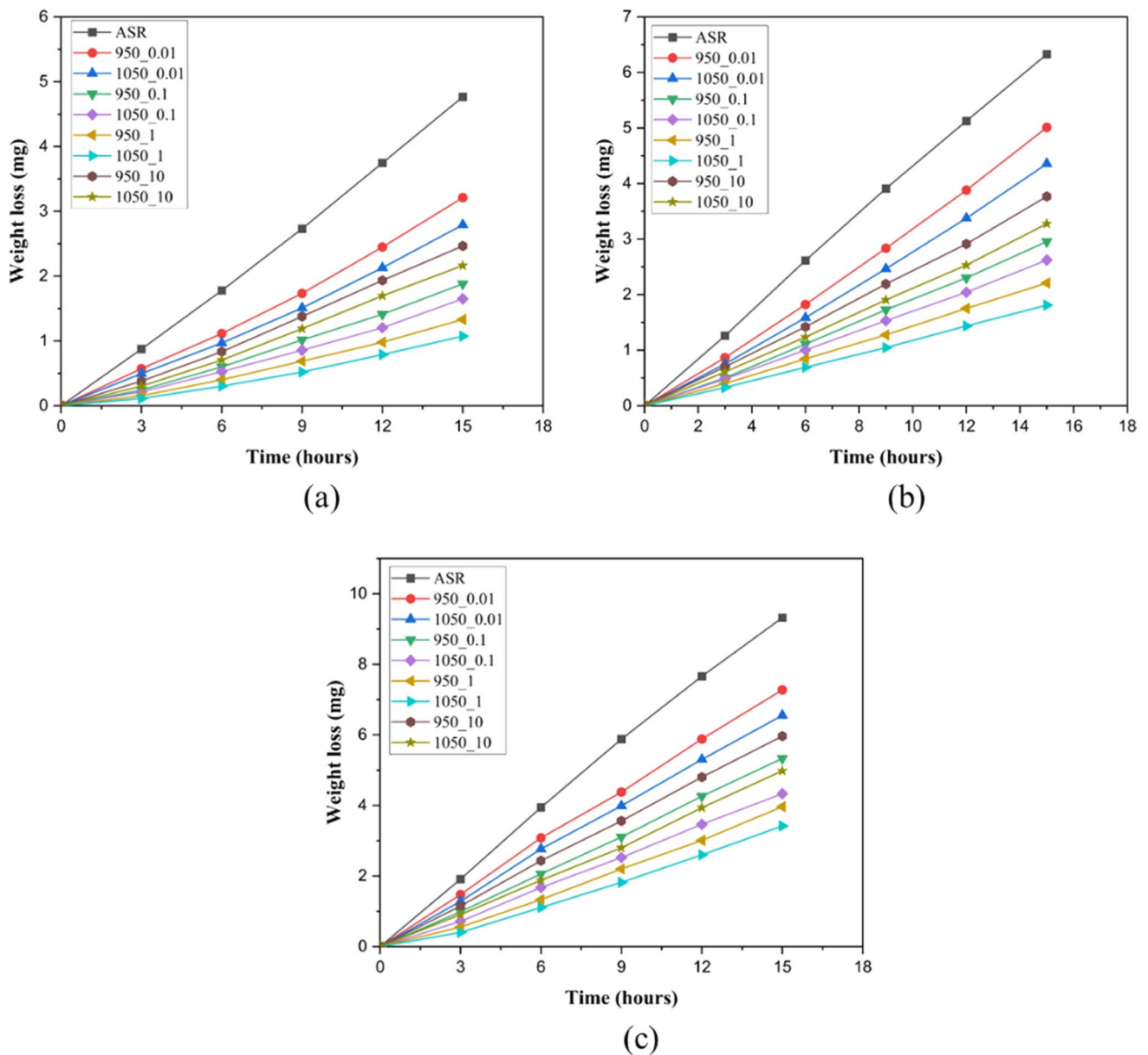
Fig. 12 Weight loss of the various specimens at 600 rpm. **a** 50%, **b** 60% and **c** 70% solid concentration (by weight)
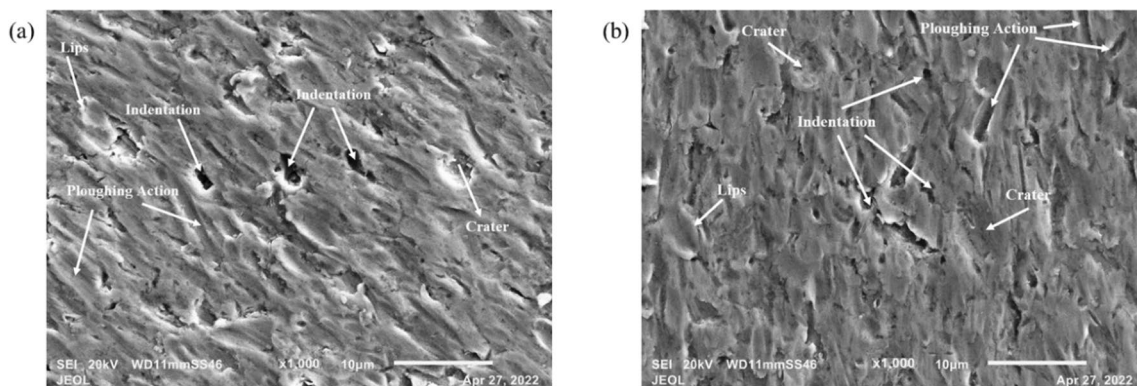

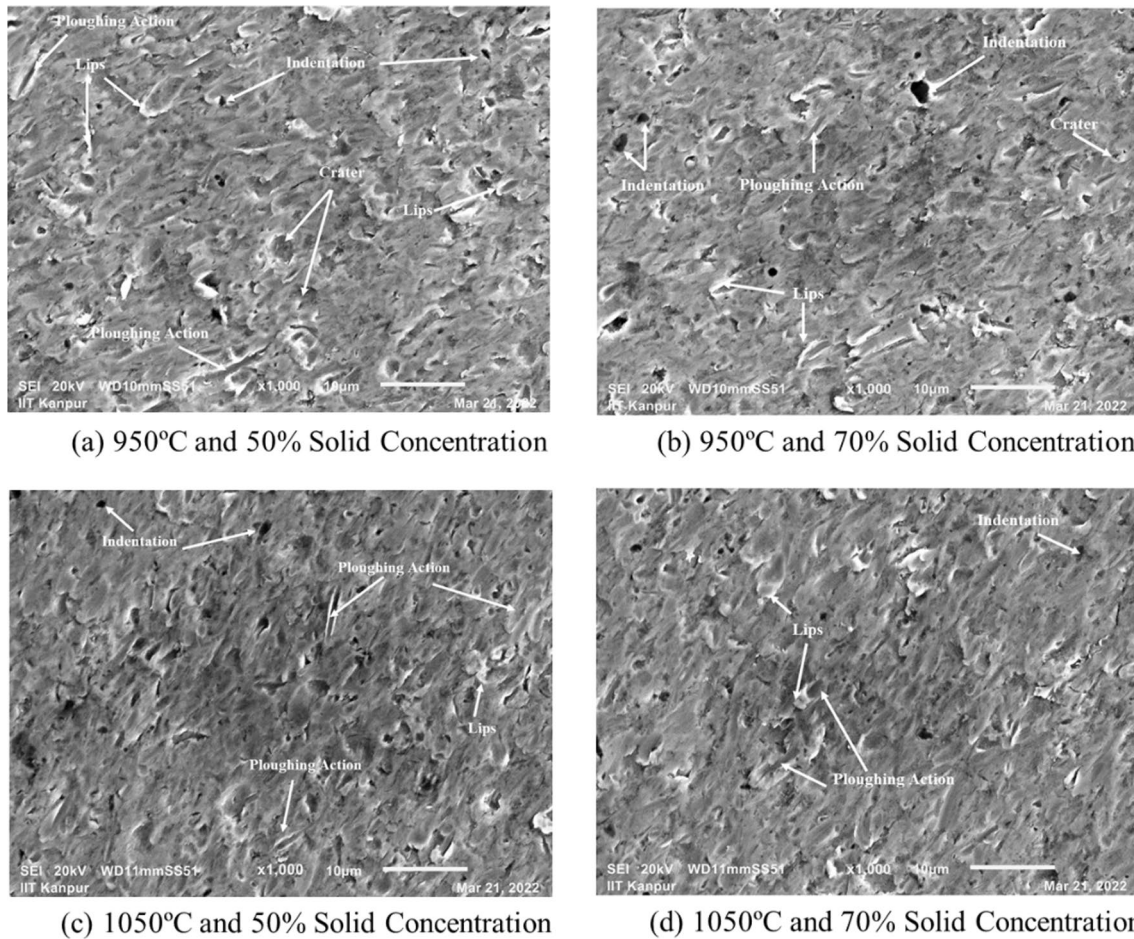**Fig. 13** SEM of the ASR specimen at 600 rpm. **a** 50% and **b** 70% Solid Concentration (by weight)

(a) 950°C and 50% Solid Concentration

(b) 950°C and 70% Solid Concentration

(c) 1050°C and 50% Solid Concentration

(d) 1050°C and 70% Solid Concentration

Fig. 14 SEM of the TMP specimen at 600 rpm and 0.01 s^{-1} strain rate

3.2 Slurry erosion wear

Figures 9, 10, 11 and 12 reported the weight loss with the test duration of as-received (ASR) and thermo-mechanical processed (TMP) specimens of SS431 at different rotational speeds and concentrations. In all cases, weight loss increases linearly with time. The highest weight loss was observed in ASR specimens; whereas, all the thermomechanical processed (TMP) specimens showed minimum weight loss compared to the ASR specimens in all cases. Due to microstructure refinement and improved mechanical properties like hardness, the weight loss of all TMP specimens is less. The weight loss is lowest for the TMP specimen when deformed at 1050 °C with a strain rate of 1 s^{-1}. At all rotational speeds and solid concentrations, the weight loss of the TMP sample (1050 °C, 1 s^{-1}) is, on average, about 75% lower than that of the ASR sample and

about 20% lower on average than that of the other TMP samples. The alteration in microstructure (finer lath and refined previous austenite grains) and increased hardness are responsible for the specimen's (1050 °C, 1 s^{-1}) TMP specimen's lowest erosion (weight loss).

In addition to that, Figs. 9, 10, 11 and 12 show the effect of rotational speed and concentration (by weight) on the slurry erosion wear, and it has been found that the weight loss of the ASR and all TMP samples increases with the rise in rotational speed and solid concentration. In all samples (ASR and TMP samples), 1.6 to 1.5 times weight loss increased with the increase in rotational speed at all concentrations; however, 2 to 1.8 times weight loss rose with the increase in solid concentration at all rotational speeds. Therefore, it is concluded from the above discussion that the slurry erosion wear is strongly dependent on the solid concentration as compared to the rotational speed.
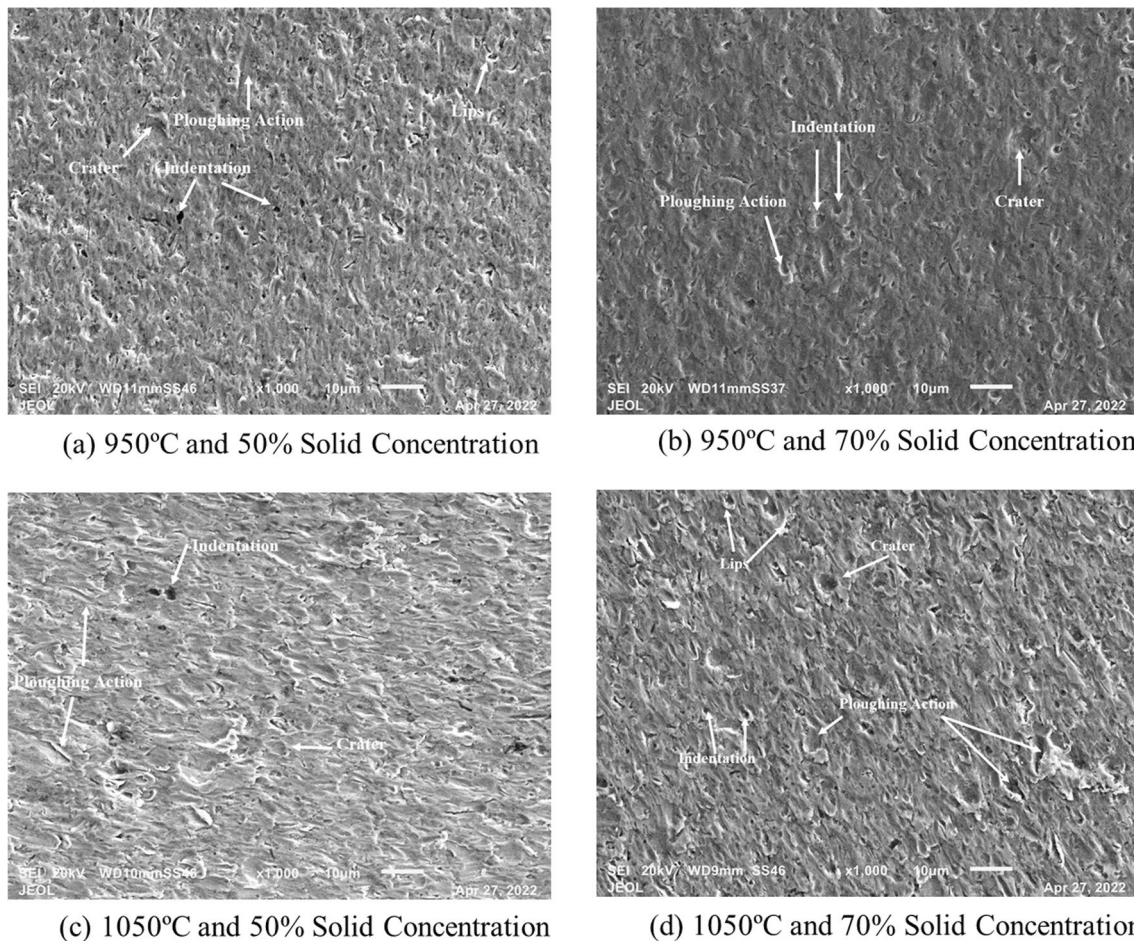
(a) 950ºC and 50% Solid Concentration

(b) 950ºC and 70% Solid Concentration

(c) 1050ºC and 50% Solid Concentration

(d) 1050ºC and 70% Solid Concentration

Fig. 15 SEM of the TMP specimen at 600 rpm and 0.1 s^{-1} strain rate

3.3 Morphology of the eroded surface of the specimens

Surface morphologies of the eroded specimens (as-received and TMP samples) have been obtained by scanning electron microscope. The morphologies of specimens have been studied near the center of the specimen. Figure 13, 14, 15, 16 and 17 shows the SEM of the ASR and TMP samples at 600 rpm and at two concentrations (50% and 70% by weight) at the end of the test. Indentation, ploughing, and crater erosion mechanisms were observed during the slurry erosion wear. It is clearly seen from the figures that the fly ash particles normally impinged on the material surface and created deep indentations and ploughing action on the surface. The Continuous impacts of fly ash particles in the center region of the specimens result in strain hardening of the eroded surface, which further leads to material loss [37, 38].

It is observed from Fig. 13 that the deeper indentations and ploughing action are present in the as-received specimen as compared to all TMP specimens at all flow parameters (concentration and rotational speed). At 1050 °C and 1 s^{-1}, the TMP specimen shows less erosion mechanisms (indentation, crater, and ploughing action) as compared to all TMP samples (all strain rates) at both concentrations (50 and 70% by weight) due to high hardness. Hence, it showed a maximum erosion resistance compared to the other specimens. The intensity of the erosion mechanism increases with the increase in both rotational speed and solid concentration [39, 40].

4 Conclusions

Temperatures of 950 °C and 1050 °C were used in conjunction with four strain rates of 0.01, 0.1, 1, and 10 s^{-1} to perform thermo-mechanical processing on SS431 martensitic stainless steel. In this work, processed and
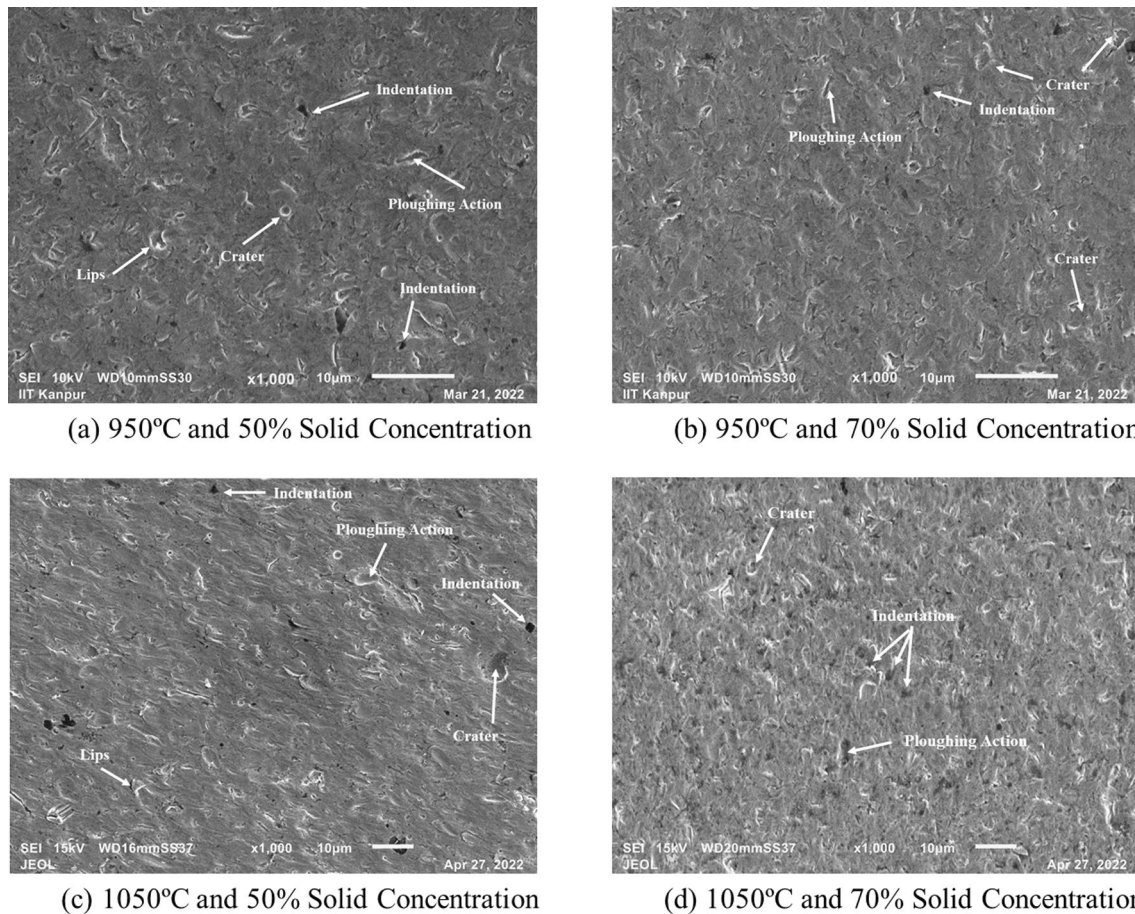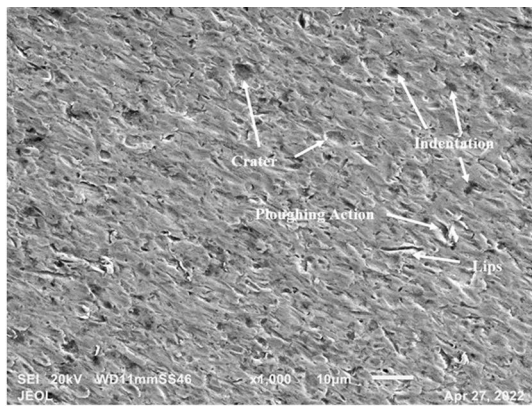
(a) 950ºC and 50% Solid Concentration

(b) 950ºC and 70% Solid Concentration

(c) 1050ºC and 50% Solid Concentration

(d) 1050ºC and 70% Solid Concentration

Fig. 16 SEM of the TMP specimen at 600 rpm and 1 s^{-1} strain rate

unprocessed SS431 materials have been analyzed and evaluated regarding their resistance to erosion by a slurry.

- In comparison with the ASR specimen, all TMP specimens have significantly smaller average grains. The TMP specimen's grain size ranged from 63 to 91 μm, which shows a significant reduction from the ASR specimen's original value of 215.15 μm.
- The TMP specimens show the highest hardness as compared to the ASR specimen. In TMP specimens, the hardness increases with the rise in deformation temperature. At 1050 °C, 1 s^{-1}, the TMP specimen shows the highest average hardness.
- Weight loss is increased with the rise in concentration and rotational speed for all the specimens (ASR and TMP specimens). It has been found that, as compared to the ASR, all TMP specimens give the least weight

loss at all flow parameters. At all rotational speeds and solid concentrations, on average, the weight loss of the TMP sample (1050 °C, 1 s^{-1}) is about 75% lower than that of the ASR specimen and about 20% lower than that of the other TMP specimen. This is due to its higher hardness and small grain size. Hence, at 1050 °C, 1 s^{-1} TMP showed the least slurry erosion wear compared to the other specimens.

- Indentation, crater and ploughing erosion mechanisms have been found on the wear surface of all specimens. In the ASR specimen, all erosion mechanisms have been observed more as compared to the TMP specimens. All erosion mechanisms increased with the rise in concentration and rotation speed of the specimens for both ASR and TMP specimens.
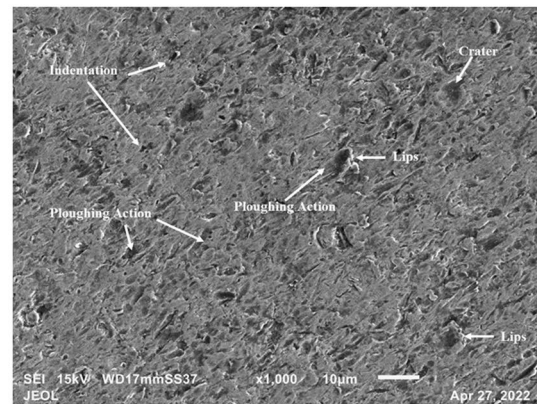
(a) 950°C and 50% Solid Concentration
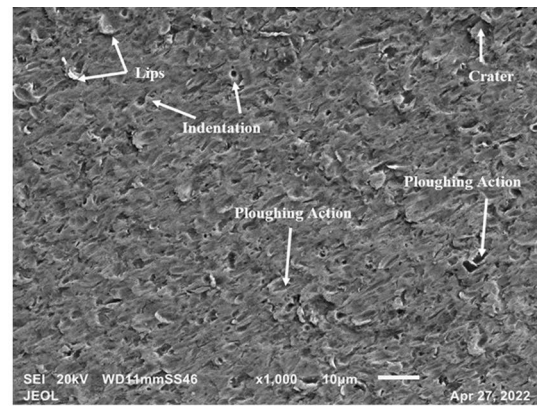
(b) 950°C and 70% Solid Concentration
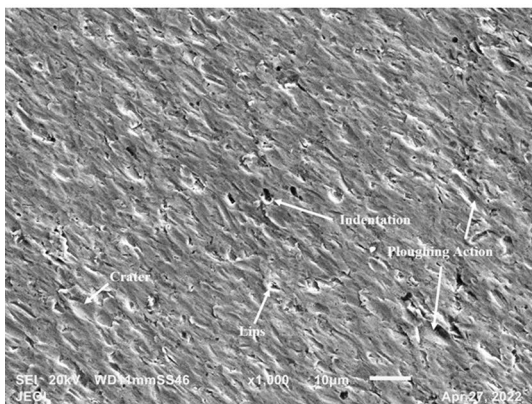
(c) 1050°C and 50% Solid Concentration

(d) 1050°C and 70% Solid Concentration

Fig. 17 SEM of the TMP specimen at 600 rpm and 10 s^{-1} strain rate

References

1. Grewal HS, Agrawal A, Singh H (2013) Slurry erosion mechanism of hydroturbine steel: effect of operating parameters. Tribol Lett 52:287–303
2. Basha SS, Periasamy VM, Kamaraj M, Shariff SM (2013) Improvement of slurry erosion wear resistance of 16Cr-5Ni martensite stainless steel by LSA and LTH. J Mater Eng Perform 22:3689–3698
3. Kumar S, Ratol JS (2013) Effects of tribological parameters on slurry erosion behaviour of uncoated and coated materials: a review. Mater Eng 20(3):119–131
4. Goyal DK, Singh H, Kumar H, Sahni V (2012) Slurry erosion behaviour of HVOF sprayed WC–10Co–4Cr and Al2O3+ 13TiO2 coatings on a turbine steel. Wear 15(289):46–57
5. Santa JF, Espitia LA, Blanco JA, Romo SA, Toro A (2009) Slurry and cavitation erosion resistance of thermal spray coatings. Wear 267(1–4):160–167
6. Chauhan AK, Goel DB, Prakash S (2008) Erosion behaviour of hydro turbine steels. Bull Mater Sci 31:115–120
7. Rajahram SS, Harvey TJ, Wood RJ (2011) Electrochemical investigation of erosion–corrosion using a slurry pot erosion tester. Tribol Int 44(3):232–240
8. Chandel S, Seshadri V, Singh SN (2009) Effect of additive on pressure drop and rheological characteristics of fly ash slurry at high concentration. Part Sci Technol 27(3):271–284
9. Amarendra HJ, Kalhan P, Chaudhari GP, Nath SK, Kumar S (2012) Slurry erosion response of heat treated 13Cr-4Ni martensitic stainless steel. Mater Sci Forum 710:500–505
10. Nguyen QB, Lim CY, Nguyen VB, Wan YM, Nai B, Zhang YW, Gupta M (2014) Slurry erosion characteristics and erosion mechanisms of stainless steel. Tribol Int 1(79):1–7
11. Santa JF, Blanco JA, Giraldo JE, Toro A (2011) Cavitation erosion of martensitic and austenitic stainless steel welded coatings. Wear 271(9–10):1445–1453
12. Grewal HS, Arora HS, Agrawal A, Singh H, Mukherjee S (2013) Slurry erosion of thermal spray coatings: effect of sand concentration. Proc Eng 1(68):484–490
13. Kumar N, Yadav U, Rathi MK (2013) To study the erosion behaviour of HVOF coating of 16Cr5Ni at the different velocity of slurry. IJSER 4(6):577–583
14. Lo KH, Cheng FT, Man HC (2003) Laser transformation hardening of AISI 440C martensitic stainless steel for higher cavitation erosion resistance. Surf Coat Technol 173(1):96–104
15. Dodds S, Jones AH, Cater S (2013) Tribological enhancement of AISI 420 martensitic stainless steel through friction-stir processing. Wear 302(1–2):863–877
16. Escobar JD, Velásquez E, Santos TF, Ramirez AJ, López D (2013) Improvement of cavitation erosion resistance of a duplex stainless steel through friction stir processing (FSP). Wear 297(1–2):998–1005

17. Grewal HS, Agrawal A, Singh H, Arora HS (2012) Cavitation erosion studies on friction stir processed hydroturbine steel. Trans Indian Inst Met 65:731–734

18. Singh J, Nath SK (2020) Improvement in mechanical properties and wear resistance of 13Cr–4Ni martensitic steel by cyclic heat treatment. Trans Indian Inst Met 73:2519–2528

19. Agarwal N, Chaudhari GP, Nath SK (2014) Slurry and cavitation erosion of HSLA steel processed by warm multidirectional forging and inter-critical annealing. Tribol Int 1(70):18–25

20. Wood RJ, Walker JC, Harvey TJ, Wang S, Rajahram SS (2013) Influence of microstructure on the erosion and erosion–corrosion characteristics of 316 stainless steel. Wear 306(1–2):254–262

21. Tilly GP (1979) Erosion caused by impact of solid particles. In: Treatise on materials science & technology, vol 13. Elsevier, pp 287–319. https://doi.org/10.1016/S0161-9160(13)70071-1

22. Torrance AA (1981) An explanation of the hardness differential needed for abrasion. Wear 68(2):263–266

23. Divakar M, Agarwal VK, Singh SN (2005) Effect of the material surface hardness on the erosion of AISI316. Wear 259(1–6):110–117

24. Oka YI, Matsumura M, Kawabata T (1993) Relationship between surface hardness and erosion damage caused by solid particle impact. Wear 13(162):688–695

25. Baghel YK, Kumar J, Kishor B, Rawat A, Patel VK (2020) Effect of hot forging on the slurry erosion wear of AISI316 and AISI410 steel. Mater Today Proc 1(26):1740–1745

26. Baghel YK, Kumar J, Patel VK (2020) Effect of surface hardness on the slurry erosion wear of AISI420 stainless steel. AIP Conf Proc 2273(1):050027

27. Kishor B, Chaudhari GP, Nath SK (2016) Slurry erosion of thermo-mechanically processed 13Cr4Ni stainless steel. Tribol Int 1(93):50–57

28. Kishor B, Chaudhari GP, Nath SK (2018) Slurry erosion behaviour of thermo-mechanically treated 16Cr5Ni stainless steel. Tribol Int 1(119):411–418

29. Momeni A, Dehghani K (2010) Characterization of hot deformation behavior of 410 martensitic stainless steel using constitutive equations and processing maps. Mater Sci Eng A 527(21–22):5467–5473

30. ASTM E209 (2010) Standard practice for compression tests of metallic materials at elevated temperatures with conventional or rapid heating rates and strain rates. ASTM Committee E28 on Mechanical Testing, West Conshohocken

31. Balan KP, Rama Rao KV, Venugopal Reddy A, Sarma DS (1999) Determination of potency factor of cobalt for estimation of nickel equivalent in 16Cr–2Ni martensitic stainless steel. Mater Sci Technol 15(7):798–802

32. Rajasekhar A, Reddy GM, Mohandas T, Murti VSR (2008) Influence of post-weld heat treatments on microstructure and mechanical properties of AISI 431 martensitic stainless steel friction welds. Mater Sci Technol 24(2):201–212

33. Rajasekhar A (2015) Heat treatment methods applied to AISI 431 martensitic stainless steels. Int J Sci Eng Res 6(4):547–553

34. Tsai WJAI, Humphrey JAC, Cornet I, Levy AV (1981) Experimental measurement of accelerated erosion in a slurry pot tester. Wear 68(3):289–303

35. Dieter GE, Kuhn HA, Semiatin SL (eds) (2003) Handbook of workability and process design. ASM international, Detroit

36. Ren F, Chen F, Chen J (2014) Investigation on dynamic recrystallization behavior of martensitic stainless steel. Adv Mater Sci Eng 2014:986928

37. Grewal HS, Agrawal A, Singh H (2013) Slurry erosion mechanism of hydroturbine steel: effect of operating parameters. Tribol Lett 52(2):287–303

38. Kumar H, Prasad R, Srivastava A, Vashista M, Khan MZ (2018) Utilisation of industrial waste (Fly ash) in synthesis of copper-based surface composite through friction stir processing route for wear applications. J Clean Prod 196:460–468

39. Gupta R, Singh SN, Sehadri V (1995) Prediction of uneven wear in a slurry pipeline on the basis of measurements in a pot tester. Wear 184(2):169–178

40. Gandhi BK, Singh SN, Seshadri V (1999) Study of the parametric dependence of erosion wear for the parallel flow of solid–liquid mixtures. Tribol Int 32(5):275–282